

WHIRC DETECTOR CHARACTERISTICS

[Return to WHIRC Home Page](#)

1. [Introduction](#)
2. [Dark Frames](#)
3. [Flatfield Frames](#)
4. [Data Processing](#)

1. Introduction

This document is intended to be a reference catalog of WHIRC images to assist the user in evaluating the performance of the instrument and to assist in troubleshooting should apparent problems occur during an observing run.

All of the images in this document were obtained after March 2008, once the default operating mode of rolling reset at a bias of 0.7 v was established. Unless specifically noted in the captions, all images were obtained using the Fowler-1 readout mode. Except for the raw frame shown in section 4, the reference pixels on the right side of the array have been stripped off.

2. Dark Frames

2.1 Typical Well-behaved Dark Frames

Dark frames are not required for normal observing, since both astronomical observations and flatfields utilize local subtraction of bias and dark current through the use of dithering (to obtain sky background) and "lights on – lights off" observations (to obtain dome flats). Nevertheless, we recommend taking a series of 10 or more short 5s darks at the beginning of the night to verify reasonable noise characteristics. The short darks presented here are the average and sigma images of ten 5s darks using the IRAF imcombine task.

NOTE: If one is generating sky flats, a series of dark exposures is required at the same integration time used for the sky observations.

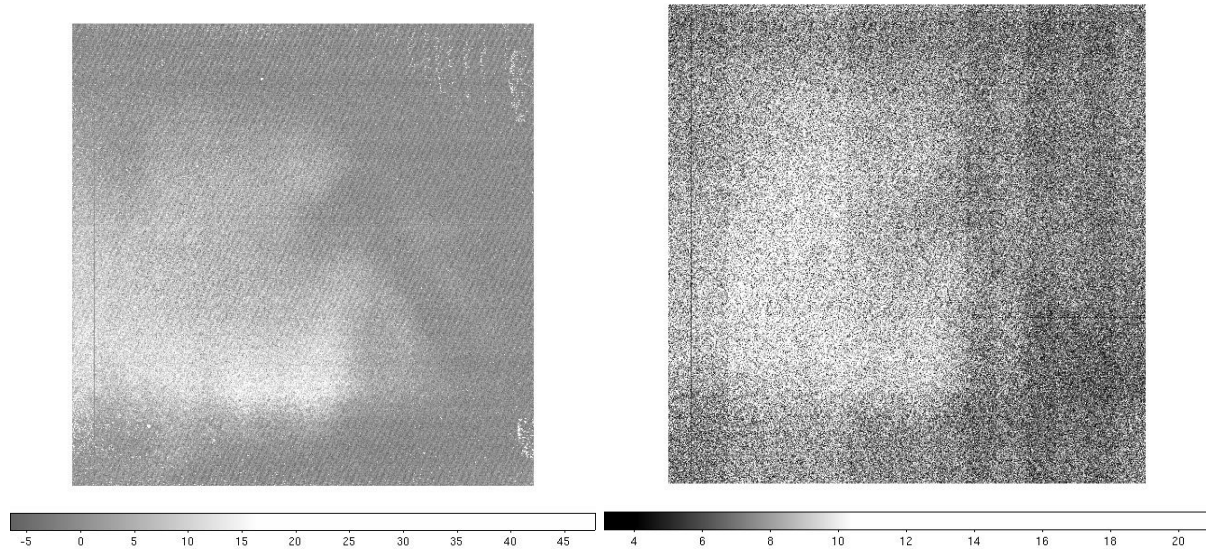


Figure 2.1: (left panel): Average of ten 5s darks generated with the IRAF imcombine task with sigmaclipping rejection. The "palmprint" on the left side of the detector and "cat scratches" in the upper right are regions of elevated dark current and hot pixels which are intrinsic to the array. The dead column 97 and row 286 are also intrinsic to the array. (right panel): Sigma image of the 10 dark frames. The elevated read noise in the region of the "palmprint" is normal. The difference in noise between the amplifier channels can also be seen.

Most of the "dark current" seen in short darks should be characterized as bias offsets or noisy pixels, since it is not proportional to the integration time, as is a "real" dark current due to thermally excited carriers or radiation leakage. A long exposure dark frame (Figure 2.2) does show a more uniformly elevated count level, although the "palmprint" region is still predominant.

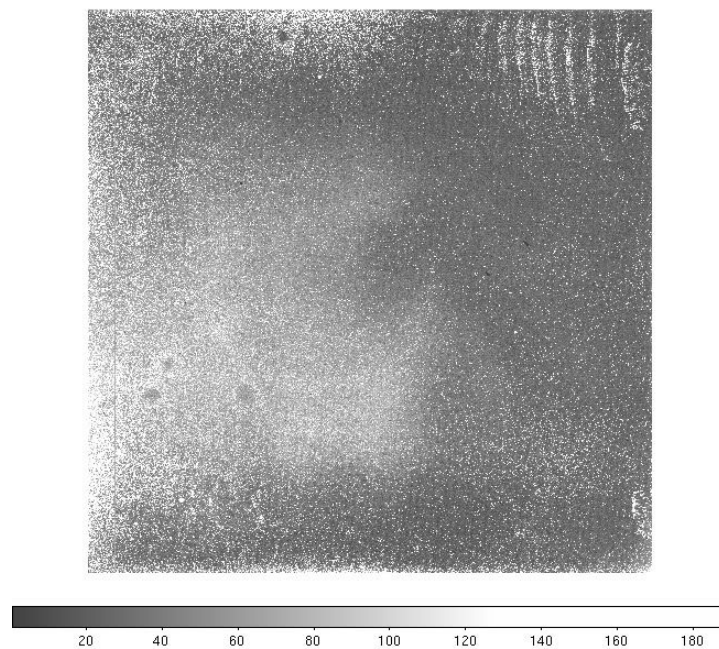


Figure 2.2: A 1000 s dark frame. The "palmprint" and "cat scratches" are still evident. The typical level ~ 80 ADU would correspond to ~ 0.27 e/s.

Tables 1 and 2 show the average and standard deviation of the mean values for seven subregions within well-behaved dark frames ranging from 4 to 1000s integration time. The values are in ADU (gain = 3.3 e/ADU), and those for Fowler-4 observations have been scaled by 0.25 to allow comparison with the Fowler-1 data.

Table 2.1: Average Signals (ADU) in Dark Frames

Time	Fowler	5:105	50:150	1415:1515	1820:1920	520:620	1670:1770	500:1500
		1925:2025	153:253	1550:1650	1050:1150	775:875	550:650	500:1500
4	1	2.39	39.22	0.72	0.60	4.00	0.61	3.01
4	1	1.81	19.18	0.71	0.45	2.62	0.58	1.76
5	1	-2.06	8.20	0.16	0.22	7.53	0.45	5.09
16	4	4.45	66.04	0.59	0.29	3.61	1.03	3.65
100	1	1.58	9.02	3.53	0.12	40.30	2.35	20.47
1000	1	58.58	137.40	25.07	33.65	88.60	38.88	50.95

Table 2.2: Sigma Values (ADU) in Dark Frames

Time	Fowler	5:105	50:150	1415:1515	1820:1920	520:620	1670:1770	500:1500
		1925:2025	153:253	1550:1650	1050:1150	775:875	550:650	500:1500
4	1	7.7	8.5	7.9	7.2	11.2	7.5	9.4
4	1	6.8	7.2	7.4	6.8	9.4	7.1	8.4
5	1	7.0	7.3	7.6	6.9	10.1	6.6	8.8
16	4	4.2	5.3	4.3	3.9	6.3	4.1	5.2
100	1	7.1	7.5	7.5	6.8	15.0	6.8	10.4
1000	1	9.9	9.4	8.7	8.4	19.0	8.7	11.7

At present, well-behaved short darks have standard deviations of the mean $\sim 7 - 9$ ADU (23 - 30 e) over the central part of the detector. The noise in the "palmprint" region is, not surprisingly, somewhat higher. The shortest possible darks with Fowler-4 readout (16 s) have readnoise in the 5 ADU (17 e) range. Figures 2.3 and 2.4 show histogram plots of the Fowler-1 and Fowler-4 images included in the tables above. *Note the smooth rolloff in the logarithmic plots at higher ADU levels; a higher ADU value for the histogram peak or a flat or peaky distribution in the rolloff is indicative of pickup or other noise problems (Figure 2.5).*

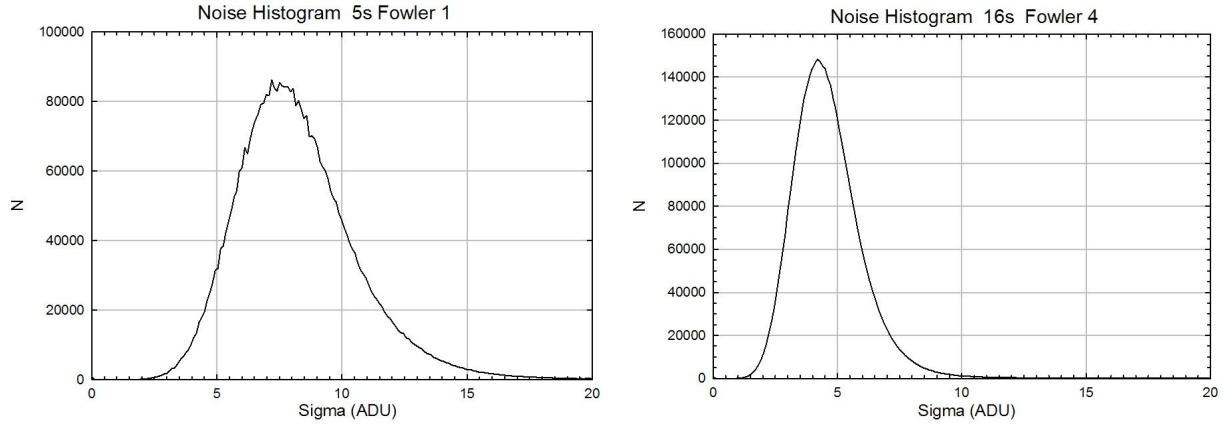


Figure 2.3: (left panel): Histogram of the sigma image of a series of 5s Fowler-1 dark frames shown in the right panel of Figure 2.1, plotted on a linear scale. The peak of the distribution is $\sim 7.5 \text{ ADU} = 25 e$. (right panel): Histogram of the sigma image of a series of 16s Fowler-4 dark frames. The ADU values were scaled by a factor of 0.25 to normalize the multiple readouts. The peak of the distribution $\sim 4.2 \text{ ADU} = 14 e$.

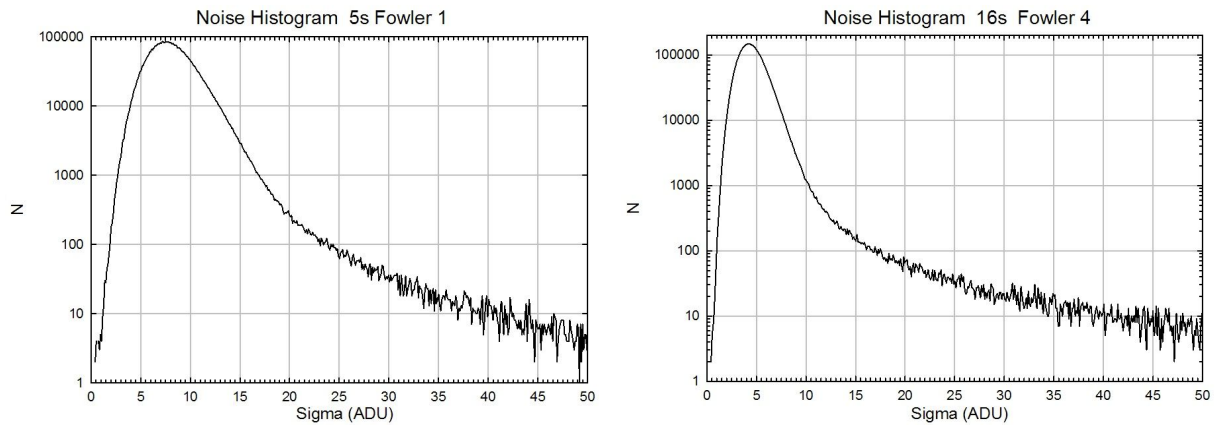


Figure 2.4: Same as Figure 2.3, except plotted on a logarithmic scale over a wider range of noise levels.

2.2 Abnormal Dark Frames

Figure 2.5 shows a short dark taken prior to the replacement of the Monsoon IR Acquisition Board, showing the periodic pattern effects from electrical pickup. *There is still some apparent periodic noise on the well-behaved dark frames (Figure 2.1), but some of this can result from aliasing between the display pixels and the detector pixels. Viewing the frames at different zoom values can often resolve this. The "Navajo rug" pattern seen in Figure 2.5 is evident at a range of display magnifications.*

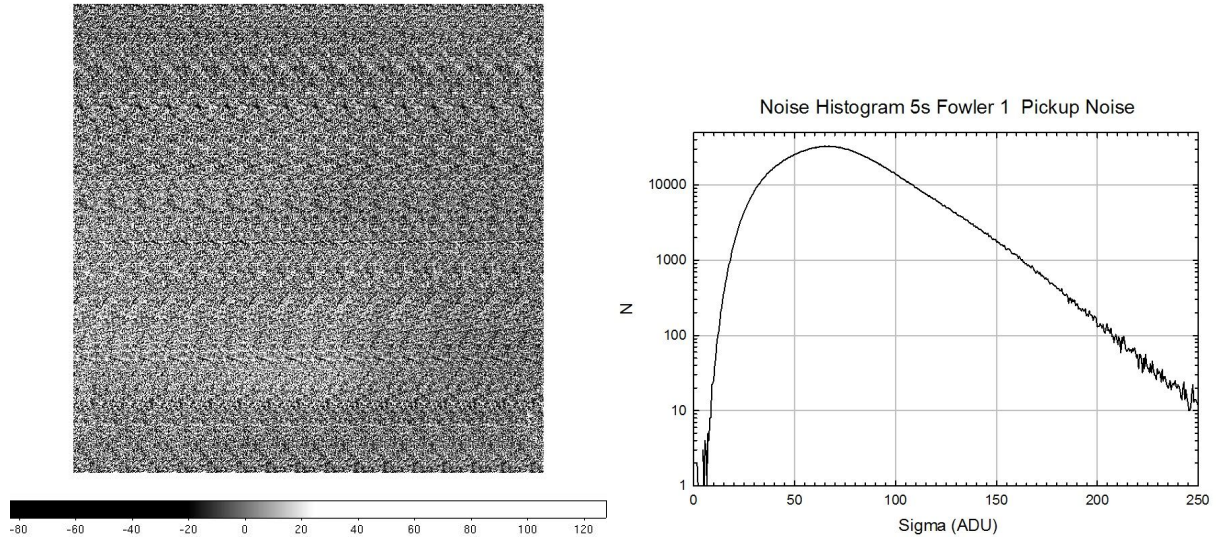


Figure 2.5: (left panel): Short dark frame showing the results of electrical pickup from the WIYN instrument rotator. Note that the high dark current from the palmprint is effectively submerged in the pickup noise. (right panel): Histogram of the sigma image of the dark frame in the left panel. Note the much higher mean value compared to the plot in Figure 2.4 as well as the slower rolloff at higher noise values.

Figure 2.6 shows a dark frame taken with the bias voltage set to 0. This can occur on initial setup if one forgets to go through the proper detector power/bias procedure, or if the built-in safety unbiases the detector after more than two hours of inactivity or the detector temperature rises above the 90 K threshold. Provided the detector temperature is in the safe zone, one may recover by running the detector power/bias routine.

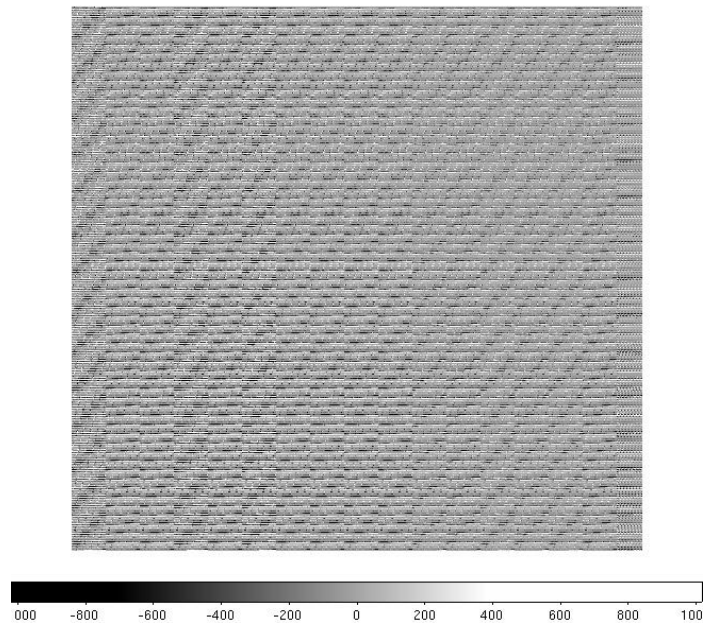


Figure 2.6: Dark frame with detector bias = 0.0. Images taken through any filter with zero bias will look similar.

3. Flatfield Frames

This section shows typical flats taken through all 13 WHIRC filters. To eliminate artifacts due to dark current, bias, or radiation background from scattered light and thermal emission from the telescope/WTTM optics, all flatfields are generated using the "lights on - lights off" observing mode. A reasonable number (10 or more) of observations are taken of the dome screen with the flatfield lights on and with the flatfield lights off. They are then processed by: 1). Trimming off the reference pixels; 2). Averaging the frames with the lights on and those with the lights off using "avsigclip" rejection; 3). Subtracting the averaged "lights off" frame from the averaged "lights on" frame; 4). Normalizing the image to a value of 1.0 using two subregions well away from the pupil ghost (vide infra)—[400:1600, 400:600] and [400:1600, 1400:1600]; 5). Replacing pixels with a value < 0.02 by 1.0 to avoid large or negative results when the flat is divided into a data image.

3.1 Common Feature Subtraction

As noted above, the use of "lights on" – "lights off" images allows one to subtract flux common to both images, leaving only the response to the flatfield lights. Because of the on-axis refractive design of WHIRC, radiation reflected from the detector and optical elements yields a false peak in the center of the detector. This "pupil ghost" is a common feature of on-axis refractive imagers and requires compensation because it does *not* represent a real response peak at the center of the field. Further information is given in the [Data Reduction Manual](#). Because of the large number of ambient temperature mirrors in the WIYN/WTTM optical train, thermal emission results in a substantial pupil ghost through filters in the K band. The pupil ghost in the "lights off" frame comes mostly from the thermal emission from the ambient temperature mirrors, so it will have a different structure and intensity than that from the flatfield lights. The subtraction of the "lights off" signal, which is substantial in the K band (Figure 3.1), from the "lights on" signal (which includes the contribution from both the flatfield light and the mirrors) is necessary to eliminate the contribution from the ambient mirrors.

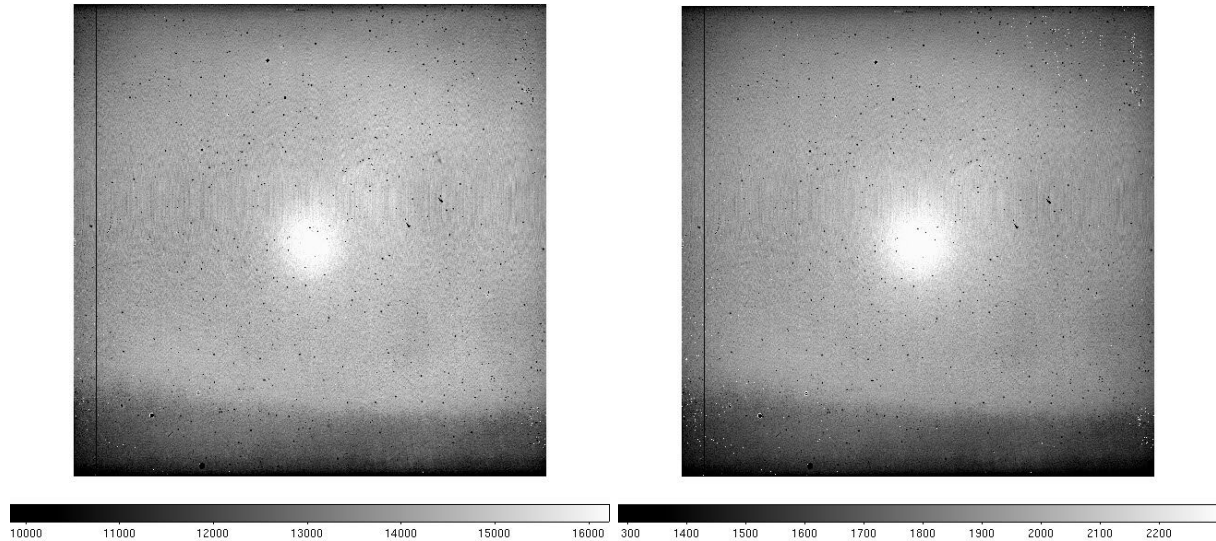


Figure 3.1: (left panel): Average of ten "lights on" frames of the dome screen taken through the Ks filter. The pupil ghost is the bright region at the center of the array. The falloff in intensity at the top and bottom of the array represents a real variation in detector responsivity. (right panel): Average of ten "lights off" frames through the Ks filter. Note that the signal is almost 15% of that with the lights on. Although it is difficult to note in these images, the pupil ghost in the "lights off" image is more extended than that in the "lights on" image. The final flat, which is generated from the difference of these two, is shown below in Figure 3.9.

3.2 Gallery of Subtracted and Normalized Flats

The processed flatfields from all 13 WHIRC filters are shown below, in order of increasing wavelength. Two normal features of these flats are the dark "fingerprint" on the upper right of the J band flats, quite possibly due to a defect in the antireflection coating on the array and the increasing prominence of the pupil ghost as one goes to longer wavelengths. These have been processed as described above to subtract out any contribution from thermal emission. Except for the features noted, the flats look pretty similar, but examples through all filters are provided for comparison to those taken at the telescope.

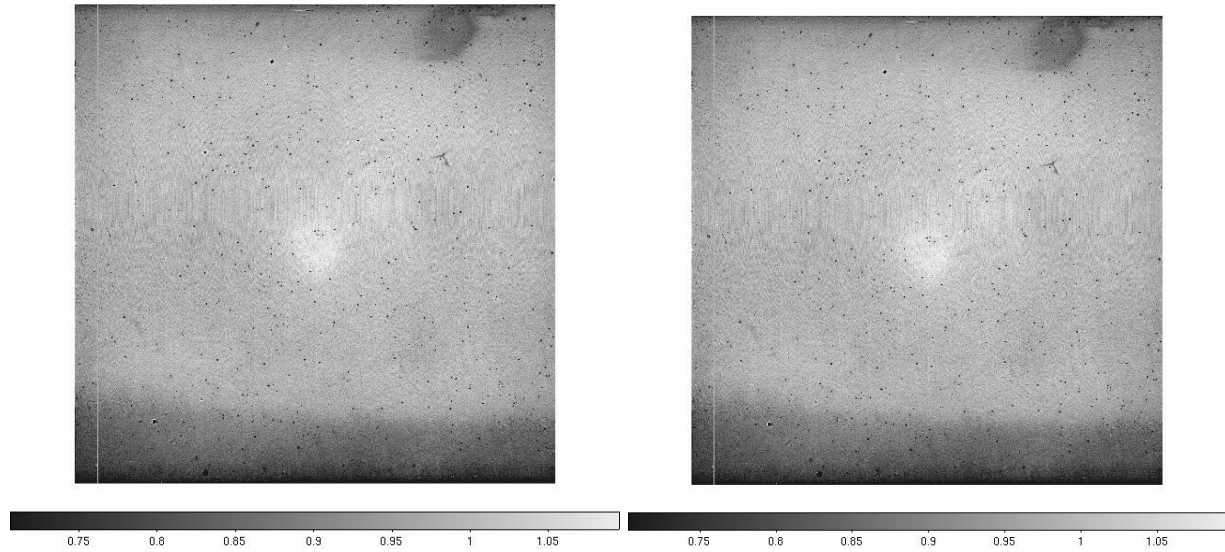


Figure 3.2: Processed flats through the 1.060 μm low airglow (left panel) and 1.082 μm He I (right panel) narrowband filters.

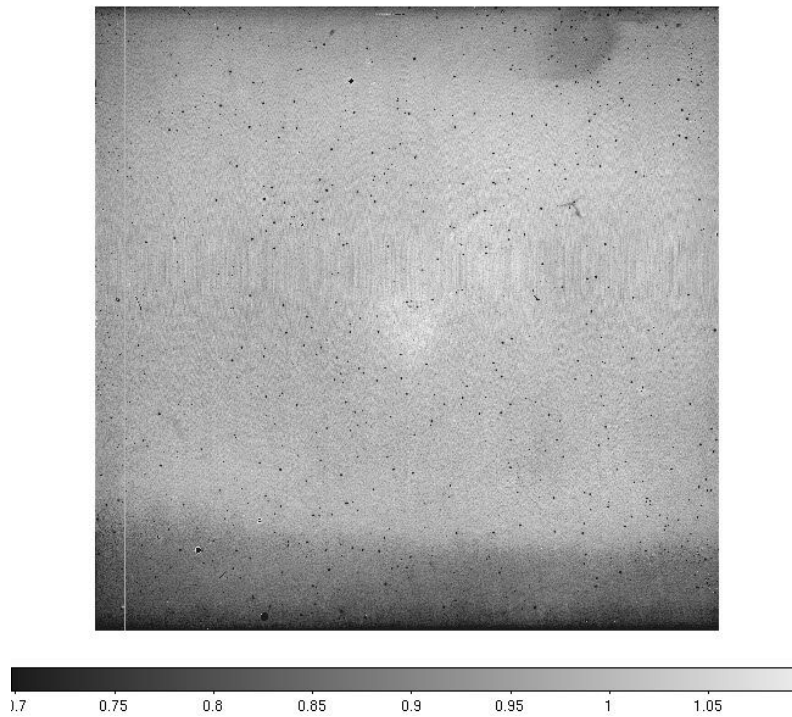


Figure 3.3: Processed flat through the 1.250 μm wideband J filter.

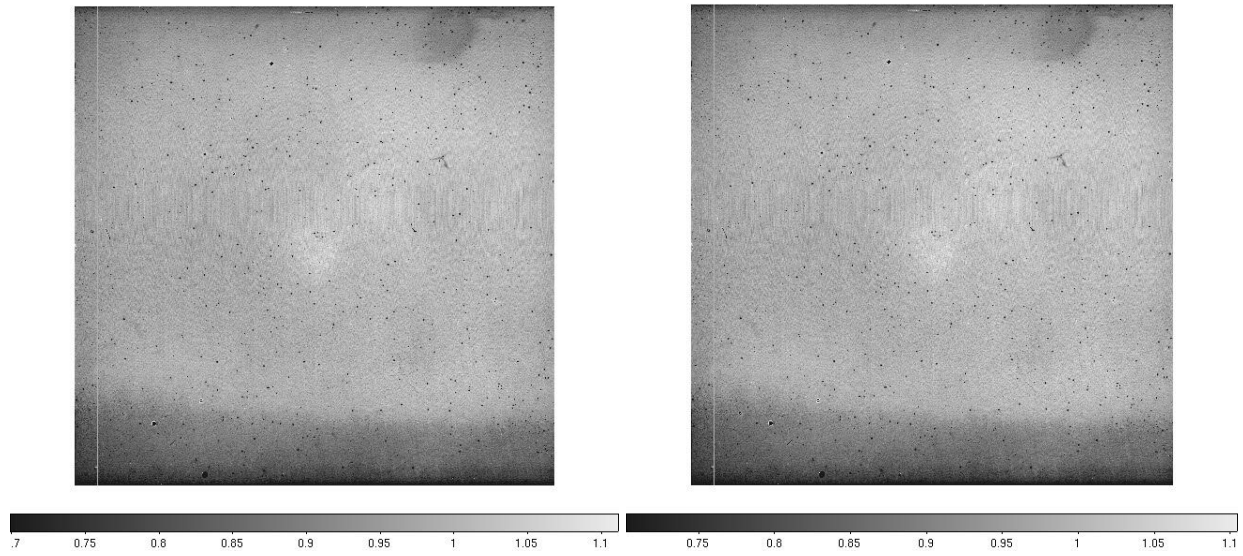


Figure 3.4: Processed flats through the 1.280 μm Pa β (left panel) and 1.303 μm Pa β 4500 (right panel) narrowband filters. Note that all of these J band filters show the "fingerprint" artifact, which appears less prominent at the longer wavelengths.

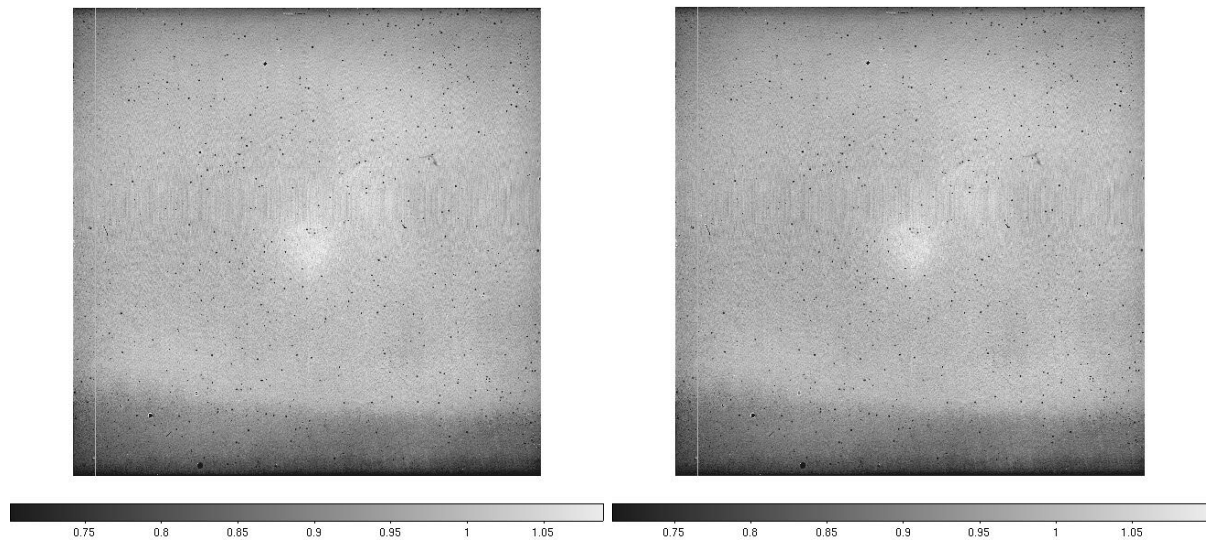


Figure 3.5: Processed flats through the 1.646 μm FeII (left panel) and 1.668 μm FeII4500 (right panel) narrowband filters. The fingerprint artifact is no longer visible.

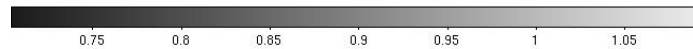
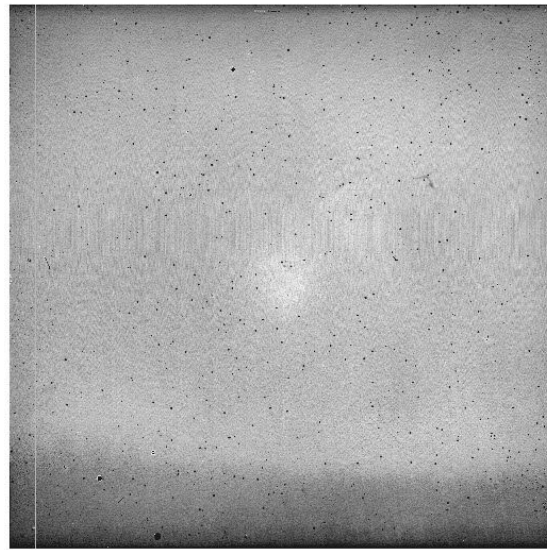


Figure 3.6: Processed flat through the 1.651 μm wideband H filter.



Figure 3.7: Processed flats through the 2.117 μm H_2 (left panel) and 2.293 μm CO (right panel) narrowband filters. The pupil ghost becomes increasingly prominent at longer wavelengths.

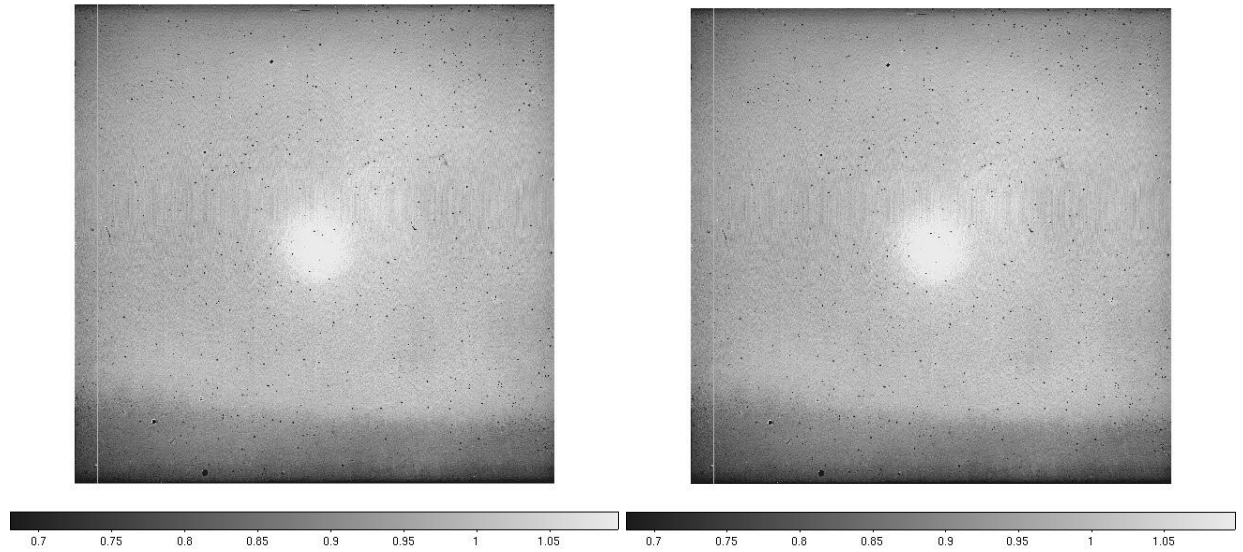


Figure 3.8: Processed flats through the 2.162 μm Br γ (left panel) and 2.188 μm Br γ 4500 (right panel) narrowband filters.

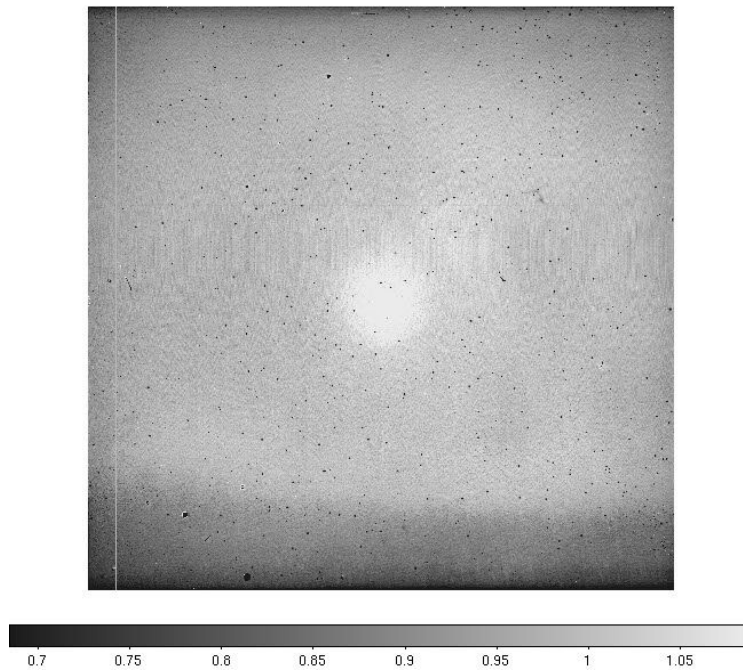


Figure 3.9 Processed flat through the 2.168 μm wideband Ks filter.

4. Data Processing

This is not meant to be a manual for data processing, but a gallery of images illustrative of the various steps in the reduction. This example is a sequence of nine images of the cluster NGC 7790 through the Ks filter taken in a 3 X 3 grid pattern with a spacing of 30 arcsec. The [Data Reduction Manual](#) covers suggested data reduction procedures in more detail.

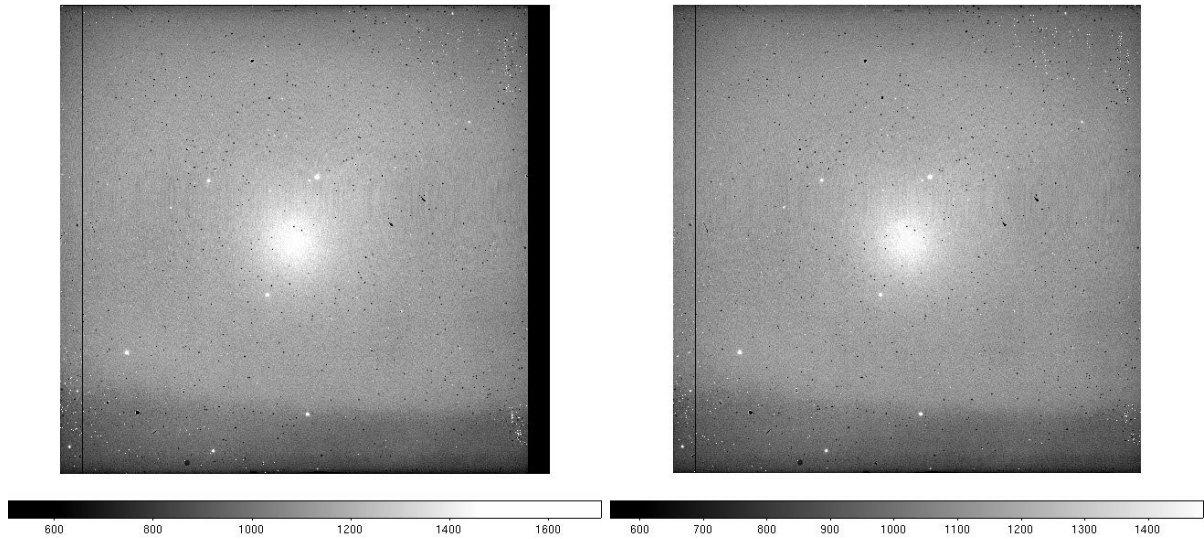


Figure 4.1: One of the nine NGC 7790 images raw (left panel) and after the reference pixels have been stripped off (right panel). Note the sky background ~ 1300 ADU in a 4 s exposure, representative of the high thermal background during the summer ($T \sim 23$ C).

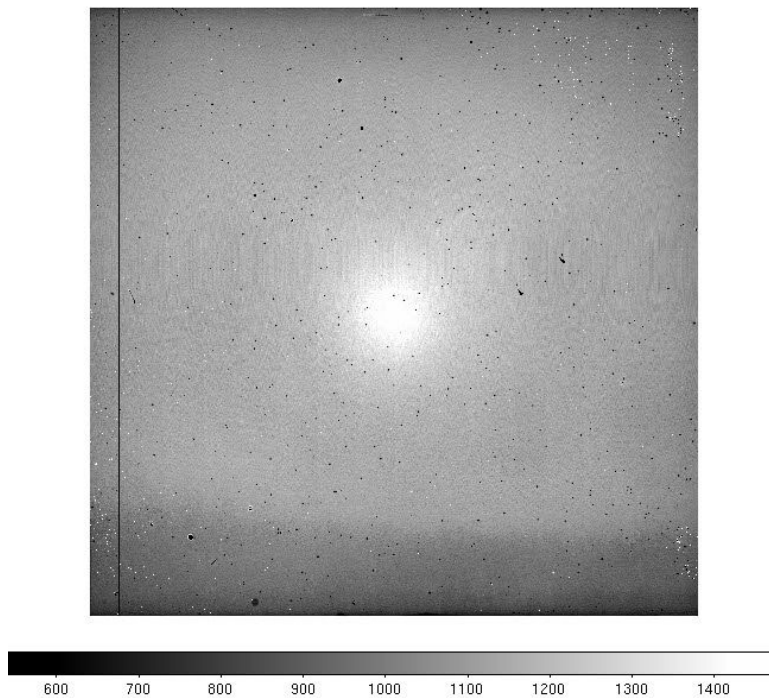


Figure 4.2 The nine trimmed images have been averaged using imcombine with a median filter. Since the stars are in different positions in each of the dithered images, they are rejected by the median filter, leaving a sky image.

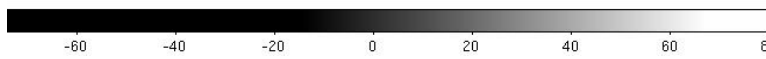


Figure 4.3 The trimmed image from Figure 4.1 after the sky frame from Figure 4.2 has been subtracted. The sky background (but not the noise from the photon statistics) has been almost eliminated.

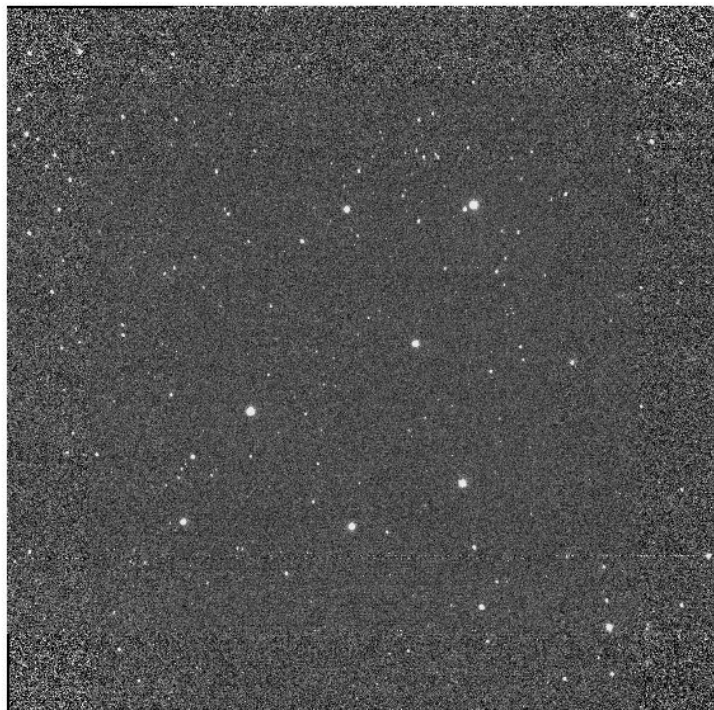


Figure 4.4: The nine sky-subtracted images have been divided by a flat (Figure 3.9), then shifted, residual sky subtracted, and combined into a single image. Note the higher sky noise in the outer portions of the image, where information from only a single image was used.